CHARACTERISTICS OF HIGH-SPEED CYCLIC TEST OF BEAM-COLUMN JOINTS

Rajesh P. Dhakal and **Tso-Chien Pan**

Abstract

The detailed procedures for high-speed cyclic loading test and the authors' first-hand experience during the tests of reinforced concrete beam-column connections subjected to cyclic displacements at frequencies as high as 20 Hz is documented in this paper. It is found necessary to give special attention to the quality of the instruments to successfully perform high-speed data acquisition. Problems faced in different phases of the high-speed tests that are not common in pseudo-dynamic tests are highlighted. The applicability of some basic criteria established for quasi-static and seismic performance in gauging the high-speed dynamic performance is also discussed. Unlike in pseudo-dynamic tests, the inertia force contributed significantly to the readings of load cells integrated with the actuators that apply the high-speed displacement cycles. The shear capacity of the tested joints was higher than that computed with the empirical equation in seismic design codes.

Keywords: beam-column joint; high-speed test; cyclic displacement; inertia effects; high-frequency signal filtering; shear capacity; failure criteria

Introduction

Reinforced concrete (RC) building frames when subjected to lateral loading may undergo severe damage in the beam-column connections or the connecting members depending on their relative strengths. The dominance of beam-column joints' contribution in the overall lateral response becomes more prominent when the building is designed to withstand the vertical dead and live loads only, as in a low seismicity region. Major sources of lateral loading in such regions where strong wind and earthquakes are not so common are underground explosion and construction vibration, which generate excitations of high frequency [Dowding 1996, Ma et al 1998]. Hence, the response of RC beam-column joints typically used in such a low seismicity region and their damage due to high-frequency excitations need to be studied and understood well in order to regulate the construction of buildings near an ammunition magazine. Even in seismic regions, the joints are designed to resist transverse actions due to low-frequency seismic ground motions, and their performances under high-frequency excitations are untested. Most of the beam-column tests conducted in the past are of quasi-static nature [Otani et al 1985, Shiohara 2001, Beres et al 1992, Hakuto et al 2000], and only a few [Agbabian et al 1994] have tested joints under actual seismic excitations. In the authors' knowledge, reports on high-speed tests of any types of beam-column joints with loading frequency representative of explosion-induced excitation are unprecedented. To provide useful information for future research, details of instrumentation, test set-up and procedures, and data acquisition scheme for high-speed tests need to be well-documented.

An extensive experimental investigation was planned to study the performance of typical reinforced concrete beam-column joints used in building frames in Singapore to high-frequency excitations, and to qualitatively and quantitatively evaluate the influence of loading rate in the overall damage of the beam-column sub-assemblies. Altogether, eight full-scale reinforced concrete beam-column joint specimens were fabricated, and cyclic loading tests ranging from slow pseudo-dynamic tests to high-speed dynamic tests were conducted in the laboratory of the National Center for Research on Earthquake Engineering (NCREE), Taiwan. As the objective of

this paper is to share the high-speed test experience and to inform researchers of the special considerations needed for similar tests, test execution and typical results of only two specimens subjected to the representative high-speed loading are discussed here.

Research Significance

As high-speed loading tests are not common, the test details and the results documented in this paper will set precedence for similar tests to be conducted for various purposes in the future. This paper aims to encourage and attract researchers to study the high-frequency response of reinforced concrete building frames. This becomes more important in moderate and low seismicity regions where some structures may not have been designed for lateral loads, and high-frequency excitations such as explosion and construction induced vibrations may pose more threat than the low-frequency seismic actions.

Specimen Details

The geometrical dimensions and cross-section details of one of these specimens are presented in Figure 1. Both specimens are of similar overall dimensions; i.e. 3.7 m high column and 5.4 m long beam. The 300×550 mm beam is reinforced with eight 32 mm diameter bars, six of them at the top and two at the bottom with a clear concrete cover of 25 mm. Similarly, the 400×400 mm column is reinforced with eight 25 mm diameter bars arranged symmetrically with clear concrete cover of 40 mm. Each beam stirrup comprises two double-legged hoops made of 10 mm diameter bars placed adjacent to each other. In contrast, each column tie consists of a single hoop of 10 mm diameter bar having three legs in the in-plane direction and two legs in the out-of-plane direction as shown in Figure 1. The beam stirrups and the column ties are spaced at 200 mm and 150 mm center to center, respectively. The beam has more reinforcing bars at the top than at the bottom, and no vertical or lateral hoops exist inside the joint core. Note that the column main bars and the beam bars at the bottom are discontinuous and are overlapped just adjacent to the joint.

The average compressive strength of the concrete taken from standard compression tests was respectively 31.7 and 33.8 MPa for the two specimens. Moreover, the average yield strengths of 32 mm, 25 mm and 10 mm diameter bars measured from standard axial tension tests were 538.0 MPa, 537.6 MPa and 363.7 MPa, respectively. Similarly, the ultimate tensile strengths of these reinforcing bars were 677.3 MPa, 675.3 MPa and 571.5 MPa, respectively. Using these material properties, section analyses were carried out to predict the failure mode of the connections. The computations revealed that both specimens are of strong-beam weak-column type, and the story shear force required to fail the column are 264.6 and 269.3 kN, respectively. The corresponding joint shear stresses computed assuming a perfect bond are 10.7 and 10.9 MPa for the two specimens. On the other hand, the empirical equation for allowable shear stress in ductile beam-column joints recommended by the ACI-ASCE seismic design code [ACI352R-91] yields 7.0 and 7.3 MPa, respectively. Similar provision in the New Zealand Standards [NZS3101-95] yields 6.3 and 6.8 MPa, respectively. These allowable values are substantially lower than the joint shear stress induced at the column failure indicating that the specimens may undergo joint shear failure before the formation of plastic hinges in the columns.

Test Set-up

To simulate the seismic action, two different loading methods are commonly found in references reporting similar beam-column joint tests. Some researchers have applied the cyclic

displacements at the column top while clamping the beam-tips [Carlos and James 2001, Otani et al 1985]. The others have applied the cyclic displacements at the beam-tips while restraining the movement of the column ends [Oka and Shiohara 1992, Filiatrault et al 1995, Beres et al 1992]. As the authors found no specific reason to prefer one arrangement to the other, the latter method was adopted in this test series; i.e. the cyclic drifts would be applied through the beam-tips rather than through the column top, because it would impose lesser disturbance on the axial load value and mechanism. Hence, each end plate of the beam was pinned to a vertical dynamic actuator, which was equipped with an internal linear variable differential transformer (LVDT) type transducer and a load cell to measure the displacement and force at the loading point. Although the column top was connected to a universal pin joint, the column was clamped to the rig at the base thus restricting the rotation and inducing a moment here. The set-up adopted in the current test series is hence different from the usual test set-ups [Hakuto et al 2000, Oka and Shiohara 1992, Filiatrault et al 1995, Carlos and James 2001, Otani et al 1985, Beres et al 1992], which use pin joints for all four supports. Because of the additional moment at the base, the proposed set-up would be statically determinate if both the forces at the beam-tip loading points and the column top are measured. Hence, an actuator integrated with a load cell and an LVDT was used to measure the horizontal reaction and displacement at the column top, in addition to the measurements of applied axial load and the reactions at the beam-tips.

The test set-up is schematically illustrated in Figure 2. Although the height and length of the specimens were 3.7 m and 5.4 m respectively, the effective height of the column is 3.2 m (distance between the centerlines of the supports at the top and the bottom) and the effective length of the beam is 6.0 m (distance between the centerlines of the actuators at the right and the left) owing to the connection details. These values were used for the conversion between absolute displacements and story drift angle, and also for the capacity predictions.

Intended Displacement History

Note the word ‘intended’ in the subtitle, which is intentionally used because the authors were not sure whether the actuators would be able to exactly follow the desired displacement history, especially during the higher-speed displacement reversals. The two specimens were subjected to two different sets of loading histories, namely normal-dynamic (ND) and high dynamic (HD). As the specimen type discussed here was identified as C4 in the overall experimental plan, the two specimens were hence named as C4ND and C4HD, respectively. Both specimens were subjected to reversed cyclic displacements with gradually increasing amplitude at the two ends of the beam through a pair of dynamic hydraulic actuators. Due to the symmetrical nature of the specimens, the displacements targeted at the two actuators at any instant were equal in amount but opposite in direction. The complete displacement history intended to apply to the connection is depicted in Figure 3. Here, the story drift angle is equal to the summation of the displacements applied to the two actuators divided by the effective beam length between the actuators; i.e. 6.0 meters.

As shown in Figure 3, the amplitude of the cyclic displacement was increased gradually in steps from 0.25% radian to 2% radian story drift angle with a 0.25% radian increment at each step. Thereafter, the increment was changed to 0.5% radian until the specimen failed. The first displacement cycle corresponding to 0.25% radian story drift angle was applied once only, and each cycle thereafter was repeated thrice. Specimen C4ND was subjected to these displacement cycles at the rate of two cycles per second; i.e. a constant frequency of 2 Hz. On the other hand, the loading in C4HD test was decided to start with 10 cycles each with ±2, ±5 and ±10 mm amplitudes applied at the fastest possible speeds. These 30 cycles were followed by the

displacement sequence shown in Figure 3, excluding the first cycle corresponding to 0.25% radian story drift angle. However, these displacement cycles in C4HD test were applied at the maximum frequencies possible with the dynamic actuator and the oil distribution system used. Consequently, the gradual increase in the amplitude of displacement cycles was accompanied by a gradual reduction in cyclic frequency. The decision on this loading pattern was inspired by the findings [Dhakal et al 2001] that lower frequency excitations correspond to lower order structural modes, for which the displacement responses are much larger than those for modes corresponding to higher frequency excitations.

As a story drift angle of 2 to 2.5% radian is thought to be a representative value to gauge the joint's seismic performance [Otani et al 1985], it was decided to temporarily halt the loading at the end of 2.5% radian story drift cycles for the first damage inspection. Thereafter, the specimen was inspected for damage after each loading step until failure. The loading in test C4HD was stopped after each of the initial high-speed small-displacement cycles to identify the crack initiation drift. Once the first crack was observed, the displacement cycles were continued until 2.5% radian story drift cycles have been applied. As the test would include planar loading, a reasonable amount of axial compression was felt necessary to prevent any undesirable out-of-plane movement of the specimen during the high-speed jerks. Hence, an axial compression was also applied at the column top through two prestressing tendons connected between the floor and a steel H beam placed at the top of the specimen. Though the axial compression was intended to keep constant throughout the loading, its value increased with the increase in the drift angle on either side. Eventually, the measured axial compression varied between 10 and 15% of the axial capacity of the column cross-section.

Instrumentation and Data Acquisition

Dynamic actuators with a capacity of ±50 ton and stroke limit of ±1000 mm were used for the high-speed loading tests. These high-velocity actuators were equipped with a servo valve capable of supplying oil at a rate of 400 gallon per minute. The relationships between the loading frequency and the displacement applicable at full load and no load are depicted in the performance curve in Figure 4. Provided that the oil supply is enough, these actuators had been calibrated to be able to apply displacement cycles of ±4 mm at a frequency of 20 Hz when no load is applied. Without mounting the specimens, the high-speed performance of the actuator was checked several times to decide the maximum frequencies at which displacement cycles of different amplitudes could be applied with sufficient accuracy. Finally, it was revealed that cyclic displacements on specimen C4HD could be applied at frequency gradually changing from 20 cycles per second (20 Hz) to 2 cycles per second (2 Hz). The initial cycles with ±2 mm, ±5 mm and ±10 mm amplitude were applied at 20 Hz, 15 Hz and 10 Hz, respectively. Similarly, the successive displacement cycles corresponding to story drift angles from 0.5% to 2.5% radian were applied at 10, 8, 7, 6, 5, 4, 4, and 3 Hz, respectively. Ultimately, the displacement cycles corresponding to story drift angle equal to and more than 3% radian were applied at 2 Hz, similar to those in C4ND test.

As the main objective of the test program was to gather information regarding the joint behavior under reversed cyclic loading at different rates, the instrumentation was mainly concentrated in the vicinity of the joint core. The overall measurement scheme included strain gauges in the beam and column main bars as well as the stirrups, a pair of pi-gauges across the joint panel and tiltmeters along the four sides of the joint. Although detailed information regarding these sensors are not relevant to the objective of this paper, it is worthy to mention that gauges and tiltmeters used must have the ability to transfer data at high-speed. As mentioned

earlier, the forces at the beam-tips and the horizontal reaction at the column top were measured with load cells integrated in the actuators, and an external load cell was used to measure the axial compression. Similarly, the displacement histories of the loading actuators and the support movement at the column top were measured with the help of LVDTs integrated in the corresponding actuators. Apart from these, a dial gauge was used to measure the bottom support movement so that the rigid body motion, if any, could be dealt with accordingly.

For data acquisition, all the strain gauges, pi-gauges, dial gauge, tiltmeters, LVDTs and load cells were connected to data loggers. Note that the conventional data loggers and connecting cables generally used in quasi-static tests are only capable of slow data transfer at the end of each pre-set displacement interval, and are not suitable to read the high-speed data at very small time intervals. Hence, a special dynamic data acquisition system was used for these high-speed tests. The data sampling frequency was set to the maximum available in the dynamic data logger, which was 200 Hz; i.e. 200 readings with 5-millisecond interval were taken in one second. The test control software was implicitly connected to and automatically recorded the data from the load cells and the LVDTs integrated in the actuators. These data were read at a higher sampling rate of 512 Hz, and enabled the crosschecking of data from the same sources recorded through the data loggers.

Performance of Specimen C4ND

As the loading was continuous, the initiation and propagation of the diagonal cracks in the joint could not be monitored until the end of 2.5% radian story drift cycles. The damage condition of both joint faces observed after 2.5% and 4% radian story drift cycles, however, are shown in Figure 5. As shown in the photographs, damage was mainly concentrated in the joint panel, and only a few cracks could be observed in the members. Cover spalling had already started in both faces of the joint at the completion of 2.5% radian story drift cycles. A few vertical cracks in the column extended to the joint in addition to the uniformly spaced flexural cracks. Beams had comparatively fewer cracks than columns did. Opening of the corners at the joint-member interface could also be noticed during the first damage inspection. The test was terminated after the cycles corresponding to 4% radian story drift angle had been applied, when the specimen showed severe damage and the story shear force degraded significantly. At this stage, concrete cover spalled off from both faces of the joint, thus exposing the main reinforcing bars inside the joint. Apart from this, concrete pieces also came out from the corners along the joint-member interfaces.

As the specimen was symmetric, and equal and opposite displacements were applied at the two beam-tips, the load-displacement relationships at both loading points were almost identical. The load versus displacement curve at one of the actuators is plotted in Figure 6(a). The maximum load corresponding to the two opposite directions are not equal because of the different amounts of reinforcement at the top and bottom of the beam. The story shear force versus story drift relationship is shown in Figure 6(b). Here, the story shear force is the load cell reading at the column top, and the story drift is the average rotation of the line joining the beam-tips from the original beam axis. Two special features that immediately attracted the authors' attention are discussed below.

Effect of Inertia Force

As can be seen in Figure 6(a), the load cell reading at the beam-tips is found to suddenly unload at the positive and negative peaks of each displacement cycle. This behaviour became more prominent during larger displacement cycles. This behaviour is due primarily to the

development of a large acceleration in the direction opposite to that of the displacement being applied. The mechanism is explained here with the help of an illustration in Figure 7. The displacement reversal at the positive peak of each cycle, for example, induces a sudden change of velocity from a positive to a negative value. Correspondingly, a negative spike will be formed in the acceleration history. Nevertheless, due to the mechanical limitation, the actuators cannot abruptly switch its movement from outward to inward direction or vice versa, and need some time in doing so. Consequently, there appears a smooth transition phase around the peaks of each displacement cycle. The maximum displacement that could be applied is hence slightly lower than the intended magnitude. As the transition phase is short, the negative acceleration induced becomes large, thus generating a significant inertia force. This opposite inertia force renders the load cell reading to drop sharply around the peaks of the displacement cycles.

Although the mechanism can be explained as above, it is difficult to separate the exact contribution of inertia force from the load cell reading. To compute the inertia force, the accelerations at the loading points should have been measured, which was unfortunately not planned as the authors could not foresee this problem. The inertia force can be obtained by multiplying the acceleration by the participating mass, the estimation of which involves a fair degree of uncertainty in the computation. To validate the above explanation, a representative correction with a reasonable approximation is shown here. The output displacement history obtained from the LVDT attached in the actuator is shown in Figure 8(a). As mentioned previously, the amplitude of each cycle is less than the intended value, and a smooth transition exists around the peaks. Figure 8(b) shows the acceleration history derived by taking the second derivative of the output displacement with respect to time. It clearly identifies spikes at the peak of each cycle in the direction opposite to the displacement being applied. The participating mass at each beam-tip comprises the mass of the connecting plate and an equivalent mass of the beam, which is difficult to estimate exactly. A few trials assuming different values in a logical range (600-1200 kg) were performed, and the corrected force versus displacement curve assuming a participating mass of 800 kg is shown in Figure 8(c). Comparison of Figure 8(c) with Figure 6(b) shows that the normal shape of force versus displacement curves could be restored after deducting the inertia force from the load cell readings.

As the column top is restrained, inertia force cannot be generated there. The reading from the integral LVDT at the column top also did not exceed 0.3 mm, indicating that the acceleration induced there during the test must have been negligible. Hence, the load cell reading at the column top was uninfluenced by the inertia force, and correctly represented the story shear force. Here, the authors were fortunate to have chosen to apply the cyclic displacements at the beam-tips rather than at the column top. Note that the authors were also forced to equip a load cell at the top support to make the system determinate. If the bottom support was pinned as in most test set-ups, the story shear force could have been derived from the forces at the two loading actuators and the load cell at the column top would not have been required. Because of the participation of the inertia force, derived story shear force would not be exact. As the story shear force is the main parameter the result interpretation revolves around, it is necessary to obtain its correct value from the measured data. Hence, regardless of the boundary condition of the test set-up, it is desirable to directly record the story shear force at the column top during a high-speed test rather than deriving it from the beam-tips forces. If the high-speed displacement cycles are applied at the column top, the inertia force must be separated from the force recorded at the column top to obtain the story shear force. However, the beam-tips readings would be free from inertia effect and may be used to derive the inertia free story shear force. As the accuracy of thus derived story shear force is not yet verified for high-speed loading cases, the authors would hence suggest to

keep the column top stationary and to apply the high-speed displacement cycles at the beam-tips, which would yield the correct story shear force from the inertia-free column top reading.

Effect of Signal Filtering

The curves shown in Figure 6 were plotted using the readings taken through a data logger. Note that similar curves in Figure 9 plotted using the data recorded automatically by the test software are significantly different from those shown in Figure 6. The plots from data by the test software are more undulated and have a sharper spike at the peak displacement of each cycle. On the other hand, the plots from the data logger readings are less zigzag and show a smoother reversal at the peaks. In trying to find out the cause, it was revealed that the default setting of the data logger filtered out frequencies higher than 10 Hz. As the frequency of small undulations seen in the test software record exceeds 10 Hz, the authors were convinced after extensive investigations that the difference was due primarily to the default setting that filtered out higher-frequency signals.

For explanation, displacement and force at one of the loading actuators and the reaction at the column top recorded by the data logger and the test software during the cycle having the maximum story shear force (the first cycle intended to induce 1.75% radian story drift angle) are plotted in Figure 10. The output displacement histories are not much influenced by the high-frequency signal filtering as a linear variation between two successive peaks was fed to the system. Nevertheless, the variation of the actuator force with respect to time was significantly affected. Note that the small undulation seen in the test software readings are of frequencies exceeding 10 Hz and hence were filtered by the data logger. As the column top is stationary, the story shear force read by the load cell there does not show much secondary undulations of higher frequencies, and is hence less affected by the filtering mechanism. However, the values of all these three parameters recorded at the peak were smaller in the data logger records, and the effect of inertia force was more pronounced in the test software records. For example, the maximum story shear force recorded through the data logger and test software were respectively 188.4 kN and 206.5 kN, and the actuator force and the average displacement at this instant were 55.5 kN and 47.3 mm in the data logger records and 31.9 kN and 50.3 mm in the test software records.

Although the correct values of the forces and displacements at the peak could be restored from the test software records, corresponding values received from the other sensors that were connected only to the data logger may not have been accurate. Note that this discrepancy would have gone unnoticed if the test software did not inherently record some of the channels or if the data logger records were not crosschecked. In quasi-static tests, this is not a problem as the displacement cycles are applied very slowly, and the undulations, if any, would never exceed 10 Hz. The authors were fortunate to discover it after the first test because the effect would be more severe for the second test where the loading frequency is higher than the filter frequency. This default filtering provision was hence deactivated during the second test to retrieve the correct values of the measured parameters at the peak of each displacement cycle through the data logger.

Performance of Specimen C4HD

The conditions of both faces of joint after the emergence of the first crack, after completion of 2.5% radian story drift cycles, and at the end of the test are shown in Figure 11. As shown in the photographs, the first pair of diagonal cracks was seen after 0.5% radian story drift (±15 mm) cycles were applied. Concrete cover spalling had already started at both faces after 2.5% radian story drift cycles. At this stage, the first pair of diagonal cracks had opened

significantly, while the other cracks remained thin. Cracks in the joint faces extended beyond the joint-column interface, and more flexural cracks could be observed in the columns than in the beams. A big piece of concrete had even spalled off from beneath the joint front face. In addition to the cracks in the joint faces and members, vertical cracks along the joint-beam interfaces could also be seen. This might be due to the alternate opening and closure at the joint corners. The specimen deteriorated quickly on further loading, and the test was terminated after 3% radian story drift (±90 mm) cycles had been applied. At the final stage, concrete cover spalled off from both faces of the joint, thus exposing the main reinforcing bars inside the joint.

The relationship between force and displacement measured by the integrated load cell and LVDT in one of the loading actuators is plotted in Figure 12(a). As explained earlier, the load cell reading decreases at the positive and negative peaks of each displacement cycle. Nevertheless, unlike in specimen C4ND, the sudden drop in specimen C4HD is significant even during the small-displacement cycles. This is because the induced inertia force is proportional to the loading rate in mm/sec rather than to the cyclic frequency in Hz. Because of a constant frequency in the C4ND test, the loading rate increased gradually with the amplitude of the displacement cycles, and so did the inertia force. In contrast, the combination of decreasing frequency and increasing amplitude in the C4HD test kept the loading rate (mm/sec) within certain range, and hence the inertia force was not much different during the small and large displacement cycles.

The story shear force versus story drift relationship is shown in Figure 12(b). Note that the curves presented in Figure 12 are plotted from the data recorded through the data logger that did not filter any high-frequency component. Consequently, some undulations in the loops and sharp reversals can be clearly identified in the curves. The data recorded through the test software were almost exactly same as the data logger records. The maximum values of the load and displacement at the peaks of different cycles recorded by the test software and the data logger were also equal. This corroborated the argument presented earlier that the difference in the data recorded from the two sources were due to the high-frequency signal filtering mechanism set as default in the data logger. Owing to the very high sampling frequency, the response showed undesired undulations that created difficulties in processing the data and locating the maximum load, which did not always appear at the peak displacement. It is hence recommended to retrieve data at a lower sampling rate that can capture the prominent frequency components with reasonable accuracy.

Comparison between the C4ND & the C4HD Test Results

The earlier prediction that the joint is weaker than the members is supported by the damage concentration in the joint panels, which eventually led to the termination of loading in both tests. Both specimens could withstand 2.5% radian story drift (±75 mm) cycles without showing any alarming sign of failure. The high-speed small-amplitude cycles did not cause any visible damage. Both specimens exhibited significant pinching behavior, and a gradual degradation of the story shear force could be observed in the post-peak region; i.e. especially after 2% radian story drift angle (±60 mm). The maximum story shear force observed in the test was 206.5 kN for specimen C4ND and 230.9 kN for specimen C4HD. This more than 10% increase in the capacity of specimen C4HD might be attributed to the strain rate effect, i.e. the increase of concrete strength due to faster loading speed. Computation assuming a perfect bond showed that the horizontal joint shear stress corresponding to the maximum story shear force is 8.3 MPa in C4ND and 9.3 MPa in C4HD, which are 20-40% higher than the allowable joint stresses recommended by the seismic design codes [ACI352R-91, NZS3101-95]. Note that the induced joint shear stress would still be higher if the bond deterioration is taken into account

[Shiohara 2001]. As the specimens did not have any stirrups inside the joint, the shear resistance must have come mainly from the concrete, and the capacity of a similar specimen with sufficient stirrups in the joint would certainly be higher. Hence, the empirical equations provided by the existing seismic design codes to predict the allowable joint shear stress may not be applicable to predict the shear capacity of joints subjected to a high-speed cyclic loading.

Figure 13(a) shows the variation of the difference in percentage between the story shear forces recorded at the peaks of the first and the third cycle with respect to the applied story drift angle for both specimens. In the C4HD test, this difference was unusually high (around 16%) in the small displacement region. On the other hand, the cyclic shear degradation in specimen C4ND was small in the pre-peak region, increased significantly around the peak displacement, and again became smaller during the large displacement region. As the shear force degradation in both specimens did not always increase with the increase in the applied drift, the failure criterion based on 20% shear degradation in three cycles [ACI318-02, NZS3101-95] may be misleading if applied to predict joint failure due to high-speed displacement cycles. The failure of specimen C4ND, for example, if defined as the point when the difference between the first and the third cycle readings is more than 20%, would occur at around 2.5% radian story drift angle. Nevertheless, the damage observed at this instant is not so severe as to suggest a failure, and the specimen could be further loaded without any instability. Figure 13(b) shows the stiffness degradation curves for both specimens. Here, residual stiffness is taken as the average of the secant stiffness at the opposite peaks of the first displacement cycle corresponding to the story drift angle. Although the initial stiffness of specimen C4ND was observed to be lower than that of the C4HD, it is difficult to draw any firm conclusions at low story drift values from this result because early stiffness is much dependent on pre-loading conditions such as shrinkage cracks. Nevertheless, the residual stiffness of both specimens was almost equal in the large-drift range. Note that the variation of residual stiffness observed in the tests is similar to that of the loading speed. As the stiffness of both specimens decreased gradually with an increase in the applied story drift and the observed damage, the residual stiffness may be an appropriate parameter to represent failure due to high-speed cyclic loading.

Conclusions

In this paper, high-speed cyclic loading tests of reinforced concrete beam-column sub-assemblies are reported. Causes and prevention of several potential difficulties that are not commonly confronted in the quasi-static tests are elaborated based on first-hand experience. The results presented also help assess the applicability of basic seismic design code provisions in predicting high-speed response of joints. Some useful outcomes of this paper are:

1. Special attention should be paid to the type of equipment used for loading as well as measurement. Dynamic data loggers with special cables capable of transmitting high-speed signals should be used. The data logger's default setting to filter out high-frequency signals should be deactivated before the test.
2. In high-speed cyclic loading tests, the load cell readings at the loading points would be affected by inertia. To obtain the correct value of the story shear force, the high-speed displacement cycles should be applied at the beam-tips, and the story shear force should be measured directly from a load cell at the stationary column top support.
3. The seismic failure criterion based on cyclic shear force degradation is not suitable to predict failure of RC beam-column joints due to high-speed cyclic loading. A failure criterion based on the residual stiffness, instead, seems more appropriate.

4. The tested specimens could stably sustain displacement cycles inducing 2.5% radian story drift angle indicating that the deformability is not a problem if a joint is to be subjected to a high-speed cyclic loading.
5. The maximum story shear force of the tested specimens corresponded to joint shear stresses that were 20-40% higher than the allowable joint shear stress recommended in existing seismic design codes, indicating the need to enhance the code provisions before applying them to predict high-speed shear capacity of joints.

Acknowledgements

The authors are thankful to Dr. Paulus Irawan and Assoc. Prof. Susanto Teng from NTU, Singapore and Prof. Keh-Chyuan Tsai from NCREE, Taiwan for their fruitful ideas that helped in planning and sorting out many problems during the project. The authors are also grateful to Dr. Ker-Chun Lin and Mr. Chui-Hsin Chen along with other NCREE staff for their tireless effort to conduct the tests. Last but not the least, the authors gratefully acknowledge the financial support from the Defense Science and Technology Agency, Singapore.

References

1. ACI (2002), *Building Code Requirements for Structural Concrete (ACI318M-02) and Commentary (ACI318RM-02)*, American Concrete Institute.
2. ACI-ASCE Committee 352 (1991), *Recommendations for Design of Beam-Column Joints in Monolithic Reinforced Concrete Structures (ACI 352R-91)*, American Concrete Institute.
3. Agbabian, M.S., Higazy, E.M. and Abdel-Ghaffar, A.M. (1994), "Experimental observations on the seismic shear performance of RC beam-to-column connections subjected to varying axial column forces", *Earthquake Engineering and Structural Dynamics*, 23, 859-876.
4. Beres, A., El-Borgi, S., White, R.N. and Gergely, P. (1992), *Experimental results of repaired and retrofitted beam-column joint tests in lightly reinforced concrete frame buildings*, Technical Report NCEER-92-0025, Cornell University.
5. Carlos, G.Q. and James, K.W. (2001), "Experimental study of reinforced concrete interior wide beam-column connections subjected to lateral loading", *ACI Structural Journal*, 98 (4), 572-582.
6. Dhakal, R.P., Pan, T.C. and Lan, S. (2001), "Qualitative assessment of structural damage due to underground explosion", *Proceedings of the Seventh International Conference on Inspection, Appraisal, Repairs and Maintenance of Buildings and Structures*, Nottingham, UK, 295-302.
7. Dowding, C.H. (1996), *Construction Vibrations*, Prentice Hall.
8. Filiatrault, A., Pineau, S. and Houde, J. (1995), "Seismic behavior of steel-fiber reinforced concrete interior beam-column joints", *ACI Structural Journal*, 92 (5), 1-10.
9. Hakuto, H., Park, R. and Tanaka, H. (2000), "Seismic load tests on interior and exterior beam-column joints with substandard reinforcing details", *ACI Structural Journal*, 97 (1), 11-25.
10. Ma, G.W., Hao, H. and Zhou, Y.X. (1998), "Modelling of wave propagation induced by underground explosion", *Computers and Geotechnics*, Vol. 22, N0. 3-4, pp.283-303.
11. NZS3101 (1995), *Concrete Structures Standard Part I- The Design of Concrete Structures*, Standards New Zealand.
12. NZS3101 (1995), *Concrete Structures Standard Part II- Commentary on The Design of Concrete Structures*, Standards New Zealand.

13. Oka, K. and Shiohara, H. (1992), "Tests of high-strength concrete interior beam-column joint subassemblages", *Proceedings of the 10th World Conference on Earthquake Engineering*, Balkema, Rotterdam, he Netherlands, 3211-3217.
14. Otani, S., Kitayama, K. and Aoyama, H. (1985), "Beam bar bond stress and behaviour of reinforced concrete interior beam-column connections", *Second US-NZ-Japan Seminar on Design of Reinforced Concrete Beam-Column Joints*, Tokyo.
15. Shiohara, H. (2001), "New model for shear failure of RC interior beam-column connections", *Journal of Structural Engineering, ASCE*, 127 (2), 152-160.

List of Figures

Figure 1. Geometrical and reinforcement details of specimens (dimensions in mm)
Figure 2. Schematic illustration of test set-up (dimensions in mm)
Figure 3. Displacement history applied to each actuator
Figure 4. Performance curve of the dynamic actuator
Figure 5. C4ND joint faces observed after 2.5% and 4% radian story drift cycles.
Figure 6. (a) Relationship between load and displacement at an actuator in the C4ND test; and
(b) Story shear force vs. story drift relationship for specimen C4ND.
Figure 7. Generation of a negative acceleration during high-speed displacement reversals
Figure 8. (a) Output displacement history at a loading actuator in the C4ND test;
(b) Acceleration history derived from the output displacement; and
(c) Actuator force vs. displacement relationship after correction for inertia force.
Figure 9. Plot of data recorded by the test software in the C4ND test:
(a) Relationship between load and displacement at an actuator in the C4ND test; and
(b) Story shear force versus story drift relationship for specimen C4ND.
Figure 10. Sample data recorded from different sources:
(a) Displacement, actuator force and the story shear force recorded by data logger; and
(b) Displacement, actuator force and the story shear force recorded by the test software.
Figure 11. C4HD joint faces observed after the first cracking, and after 2.5% and 3% radian story drift cycles.
Figure 12. (a) Relationship between load and displacement at an actuator in the C4HD test; and
(b) Story shear force vs. story drift relationship for specimen C4HD.
Figure 13. (a) Reduction of story shear force in three cycles; and
(b) Degradation of average stiffness with story drift.

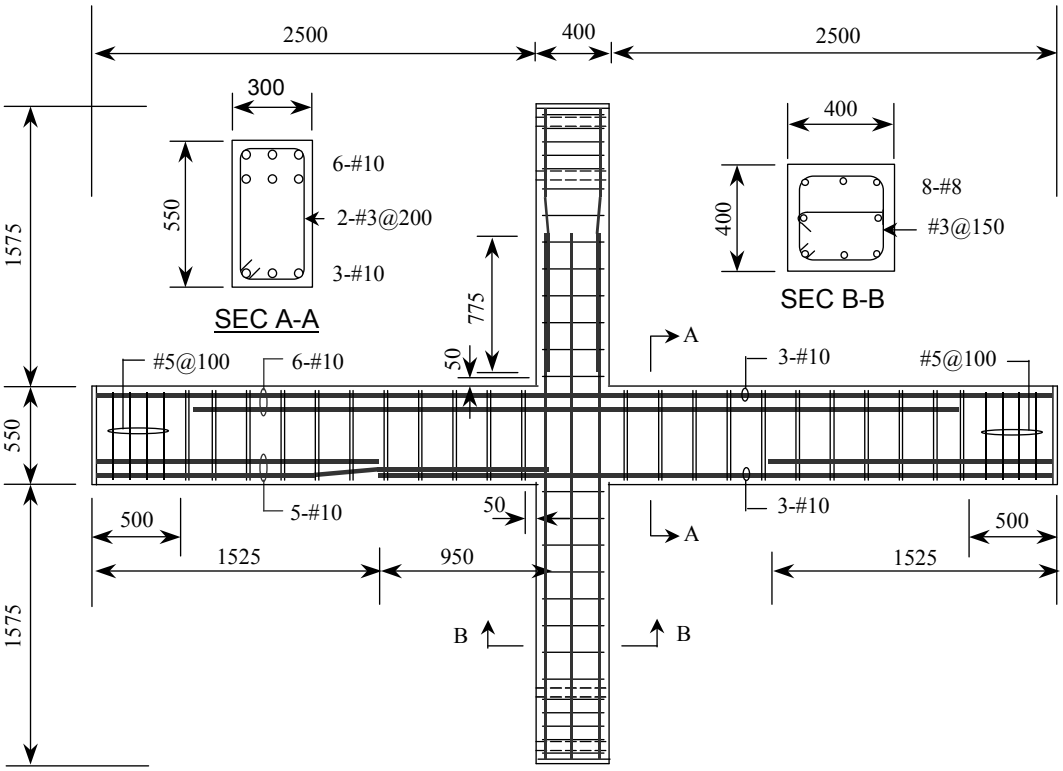
2500
400
2500
300
400
6-#10
2-#3@200
3-#10
550
1575
SEC A-A
775
50
400
8-#8
#3@150
SEC B-B
A
#5@100
6-#10
3-#10
#5@100
550
5-#10
50
3-#10
500
500
1525
950
1525
1575
B
B

Figure 1

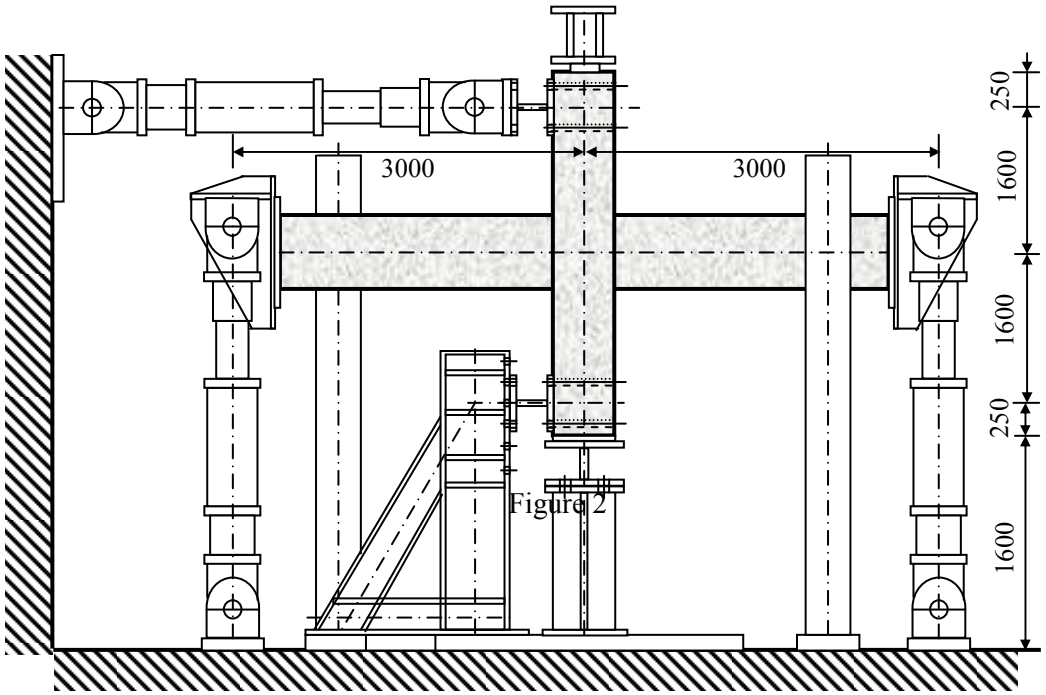

Figure 2

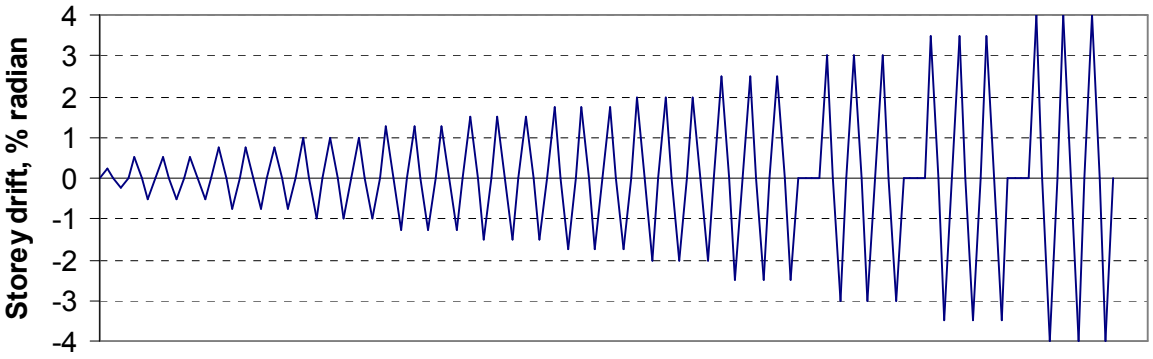

Figure 3

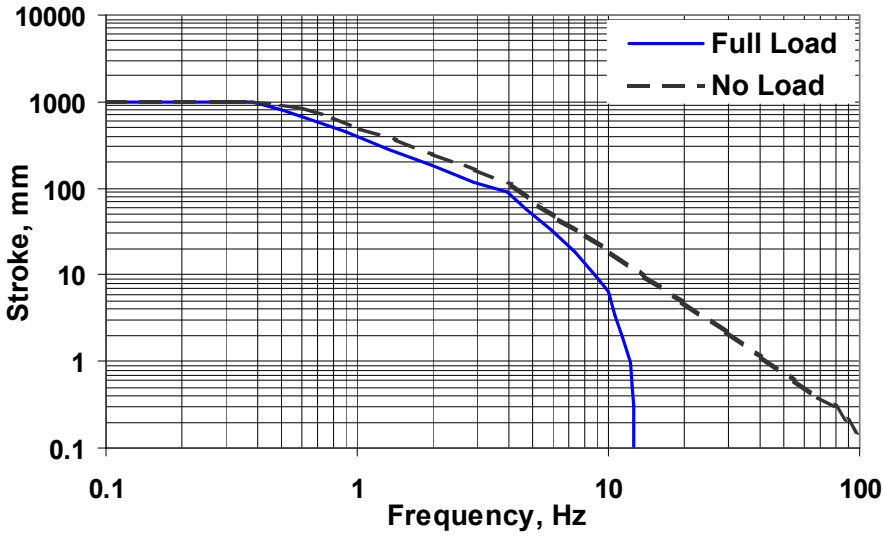
10000
1000
100
10
1
0.1
Stroke, mm
0.1
1
10
100
Frequency, Hz
Full Load
No Load

Figure 4

Figure 5

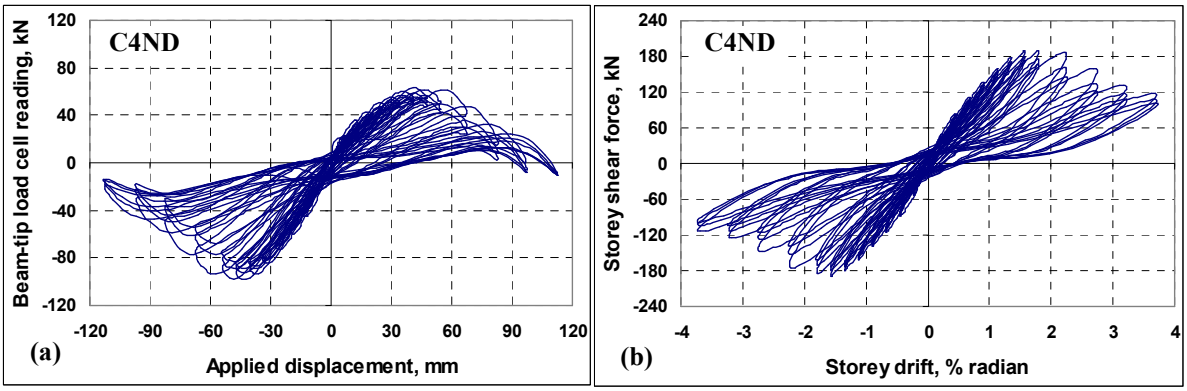
C4ND
Beam-tip load cell reading, kN
120
80
40
0
-40
-80
-120
-120 -90 -60 -30 0 30 60 90 120
(a)
Applied displacement, mm
C4ND
Storey shear force, kN
240
180
120
60
0
-60
-120
-180
-240
-4 -3 -2 -1 0 1 2 3 4
(b)
Storey drift, % radian

Figure 6

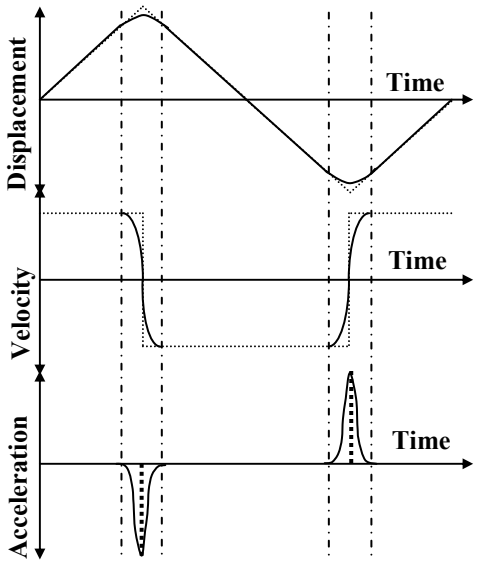

Figure 7

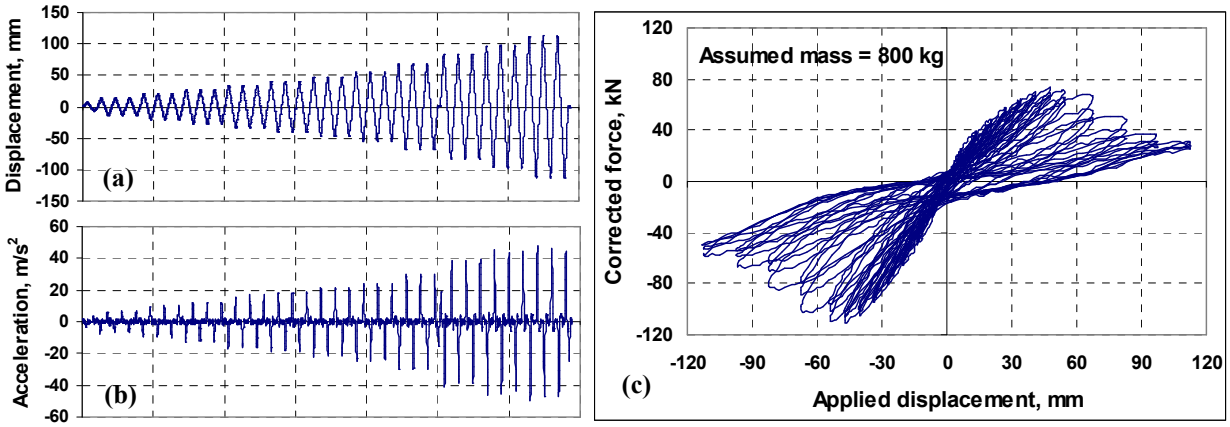
Displacement, mm
150
100
50
0
-50
-100
-150
(a)
Acceleration, m/s2
60
40
20
0
-20
-40
-60
(b)
Assumed mass = 800 kg
Corrected force, kN
120
80
40
0
-40
-80
-120
-120
-90
-60
-30
0
30
60
90
120
(c)
Applied displacement, mm

Figure 8

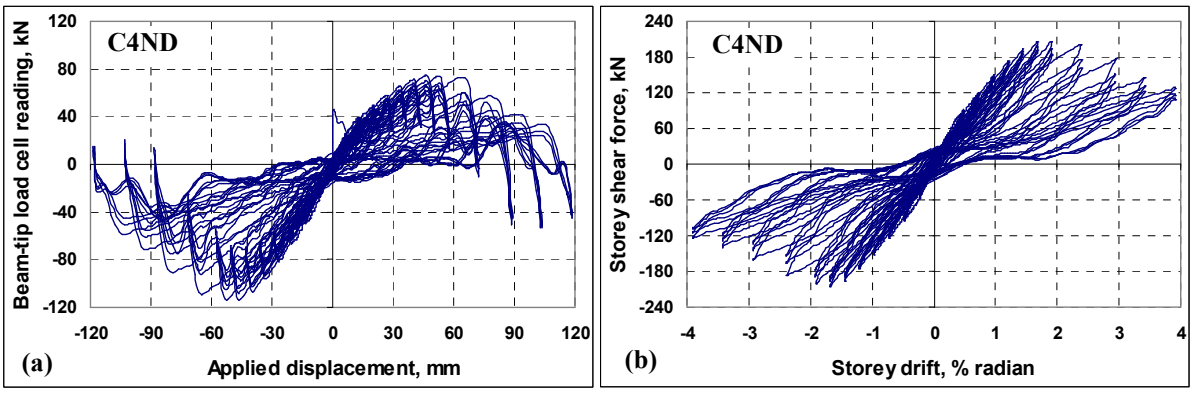
C4ND
Beam-tip load cell reading, kN
120
80
40
0
-40
-80
-120
-120 -90 -60 -30 0 30 60 90 120
(a)
Applied displacement, mm
C4ND
Storey shear force, kN
240
180
120
60
0
-60
-120
-180
-240
-4 -3 -2 -1 0 1 2 3 4
(b)
Storey drift, % radian

Figure 9

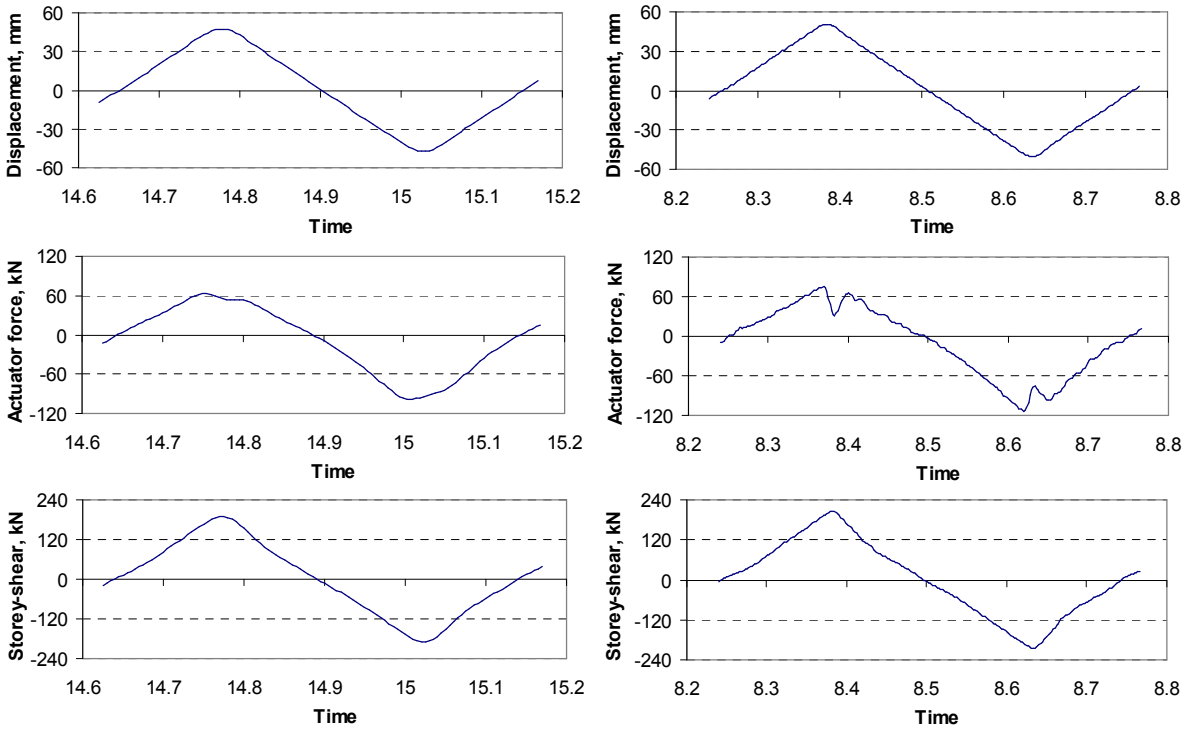

Data logger readings

Test software readings

Figure 10

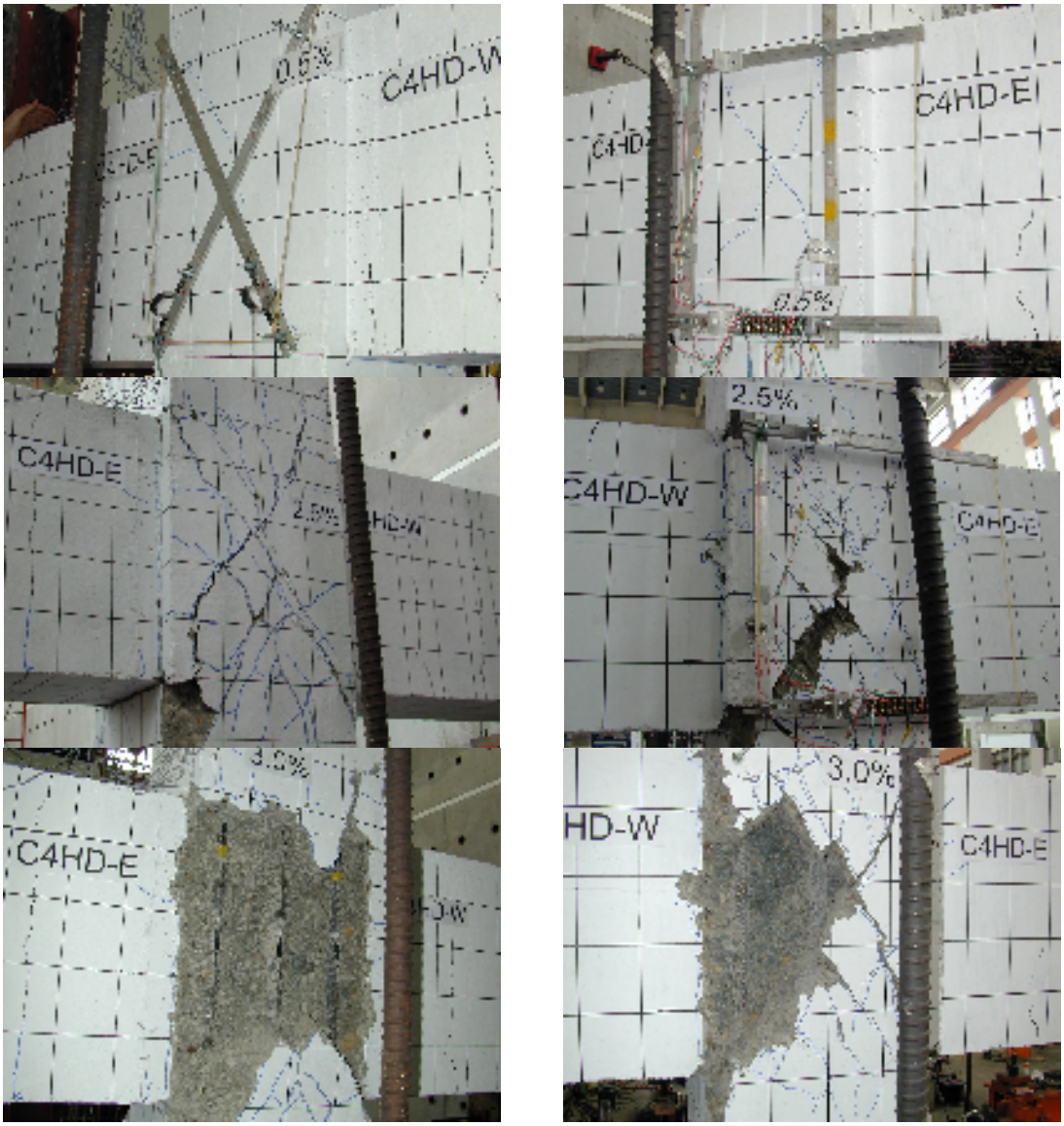

Figure 11

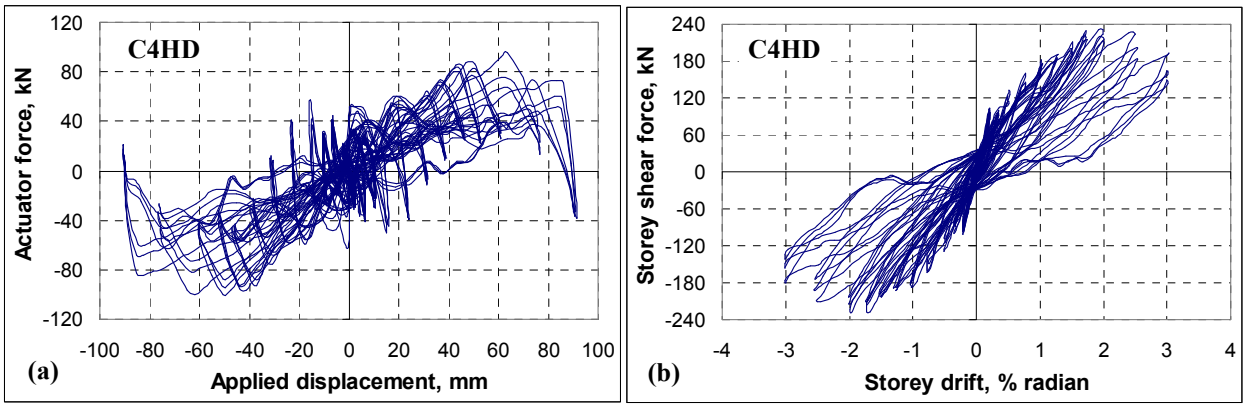
C4HD
Actuator force, kN
120
80
40
0
-40
-80
-120
-100 -80 -60 -40 -20 0 20 40 60 80 100
Applied displacement, mm
(a)
C4HD
Storey shear force, kN
240
180
120
60
0
-60
-120
-180
-240
-4 -3 -2 -1 0 1 2 3 4
Storey drift, % radian
(b)

Figure 12

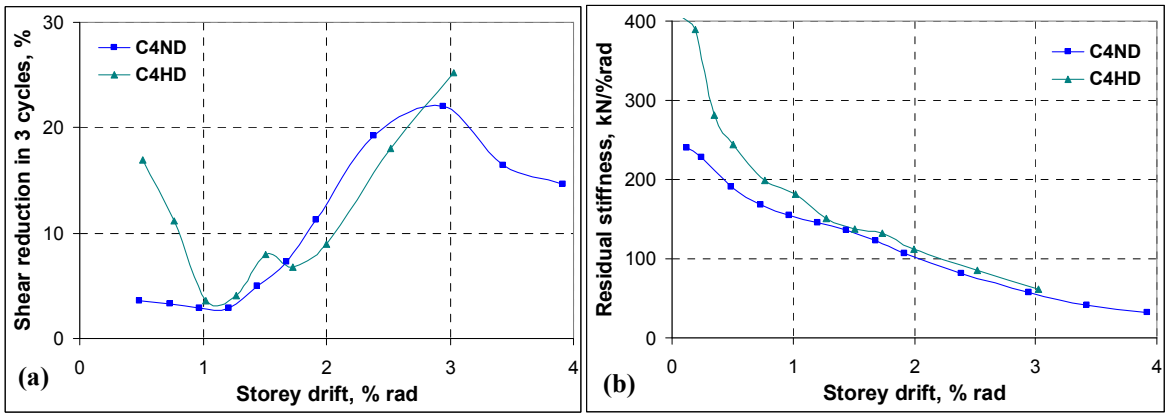
Shear reduction in 3 cycles, %
30
20
10
0
C4ND
C4HD
0
1
2
3
4
Storey drift, % rad
(a)
Residual stiffness, kN/%rad
400
300
200
100
0
C4ND
C4HD
0
1
2
3
4
Storey drift, % rad
(b)

Figure 13